

# Jamming of Cellulose Ether Solutions in Porous Medium

Claire Marlière, Paméla Faure, and Philippe Coussot

Laboratoire Navier, Université Paris-Est, Champs sur Marne, France

Dimitris Vlassopoulos

Institute of Electronic Structure and Laser, FORTH, Heraklion, Crete, Greece

Dept. of Materials Science and Technology, University of Crete, Heraklion, Crete, Greece

Antje Larsen and Benoit Loppinet

Institute of Electronic Structure and Laser, FORTH, Heraklion, Crete, Greece

DOI 10.1002/aic.14920

Published online July 14, 2015 in Wiley Online Library (wileyonlinelibrary.com)

*The flow of aqueous cellulose ether solutions through a bead packing is investigated using magnetic resonance imaging and filtration measurements. A rather complex behavior dominated by jamming (clogging) and unjamming phenomena in time is observed. With the help of several characterization techniques (laser grain sizing, dynamic light scattering, optical microscopy, and rheometry), we find that the particular methyl(hydroxyethyl) cellulose prepared with a specific protocol, tends to form aggregates in water, even at the lowest achievable concentration. These aggregates are highly polydisperse, ranging from 100 nm to 100  $\mu$ m in size, and are deformable. Their origin appears to be the hydrophobic links among molecules and the related local crystallization. It is suggested that these features play a key role in the observed jamming/unjamming during filtration tests. © 2015 American Institute of Chemical Engineers AICHE J, 61: 3923–3935, 2015*

**Keywords:** cellulose ether, porous media, suspensions, polymer properties

## Introduction

Cellulose derivatives such as cellulose ethers (CEs) are widely used as emulsifiers, thickeners, adhesives, hydrogels, and superabsorbents, in many fields such as food, pharmaceutical, personal hygiene, and building material industries. Concerning the latter, they are also used as “water retaining agents”: they limit the loss of water which results from absorption into the substrate, say during curing stage of cement formation; this improves cement hydration and its mechanical properties. CEs find applications also as viscosity-enhancing admixtures, and previous studies suggested that the increase of the interstitial solution viscosity thanks to their presence could be the cause of a better retention.<sup>1,2</sup>

Such properties may be due to specific features of these solutions or to some interactions with the solvent medium in which they are dispersed. In both cases, the physicochemical characteristics of the components of the solution play a major role. For example, a significant influence of the polymer molecular parameters like molecular weight and substitution degrees was evidenced.<sup>3</sup> These characteristics are *a priori* well known from the existing knowledge in the field of polymers. When dispersed in dilute solution in water, which is considered a good solvent, such polymers should adopt a swollen Gaussian coil conformation. The exact form of CE in solu-

tion remains debatable. For dilute solutions, the radius of gyration can be expressed as:  $R_g = K_{R_g} M_w^v$ , where  $K_{R_g}$  and  $v$  are constants which depend on the polymer structure. In fact, the same should hold for the hydrodynamic radius  $R_h$ . The intrinsic viscosity  $[\eta] = \lim_{c \rightarrow 0} \frac{\eta - \eta_s}{\eta_s c}$  (where the subscript  $s$  refers to the solvent and  $c$  is the concentration) can then be linked to the polymer molar mass  $M_w$  (here considering its weight-average) thanks to the Mark–Houwink–Sakurada equation<sup>4</sup>:  $[\eta] = K_\eta M_w^a$ , in which  $K_\eta$  and  $a$  are parameters depending on the polymer structure. This provides a general way for estimating the polymer molar mass and then deducing the radius of gyration. The values of the parameters ( $K_{R_g}$ ,  $v$ ,  $K_\eta$ , and  $a$ ) have been empirically established by Clasen and Kulicke<sup>5</sup> for different cellulose derivatives (Methylcellulose, Hydroxypropyl methyl cellulose, hydroxyethyl methyl cellulose). For semidilute solutions of CE, the solution viscosity was found to increase significantly, due to coil interpenetration and eventual formation of a physical entanglement network.<sup>6</sup>

The above approach generally leads to radius of gyration of the order of several tenths of nanometers. However, it is often the case that a true molecular dissolution of CE is not possible; instead, aggregates are formed even at very low concentrations, a feature which we shall discuss below in detail. Conversely, Bülchen et al.<sup>6</sup> suggested that water retention is enhanced by the formation of CE agglomerates of the order of several microns which, because of their large size, physically plug the pores of the cementitious matrix. Such an interpretation seems consistent with the observation of an accumulation of CE at the interface with the substrate in tile adhesives

Correspondence concerning this article should be addressed to P. Coussot at philippe.coussot@ifsttar.fr.

mortars by Jenni et al.<sup>7</sup> At last, it was shown that the data from filtration tests may be correlated with data from water retention tests, which was explained by the probable presence of aggregates in suspension.<sup>8</sup> Therefore, the presence of aggregates may be unavoidable but also beneficial for some applications. Nevertheless, characterizing the CE used in a particular process can help understanding it and optimizing it.

From the above, it is evident that, given the complexity of CE, a link between molecular characterization and macroscopic properties, which at the moment is missing, will help optimizing their behavior in various applications. In this work, we address this challenge. Here, we characterize CE elements in water from a succession of tests and analyses using light scattering, microscopy, and mechanics. In particular, we study the flow of aqueous solutions in porous media and at the same time characterize them by various techniques. We conclude that a kind of jamming occurs during such flows as a result of some accumulation of aggregates. We then attempt at qualitatively associating the observed flow phenomena with the results of the characterization, that is, the formation of poly-disperse aggregates. The manuscript is organized as follows: we first present that particular CE used and the experimental methods and means of analysis. The next section shows and discusses the various experimental results, whereas afterward we attempt at providing a tentative picture linking characterization and flow response. Finally, the main results are summarized in the last section.

## Materials and Procedures

### Materials

Unless otherwise specified, the solutions were prepared in distilled water. The CEs used were methylhydroxyethyl cellulose (MHEC) with commercial name Tylose MH 100000 P6, supplied by SE Tylose GmbH (Shinetsu). Their average degree of substitution (DS), that is, the average number of substituent groups attached per base anhydroglucose unit is 1.5 (it ranges between 0 and 3). This means that on average half of the —OH groups have been grafted with hydrophobic groups. The molar degree of substitution (MS), that is, the average number of substituted groups per anhydroglucose unit, is 0.15. CEs are water-soluble at room temperature but will phase separate and may gel thermoreversibly at temperatures above the lower critical solution temperature (LCST).<sup>9</sup> Simple turbidity measurements with the present CE aqueous solution at 0.34% wt, revealed a LCST around 35°C, conforming to literature reports.<sup>10</sup> However, CE dissolution is slow. To reduce the time of hydration and limit the formation of powder lumps, we followed a strict protocol which is industrially relevant and recommended by Shinetsu, Dow, and Saint Gobain: we first dispersed the CE white powder in hot water ( $T \sim 60^\circ\text{C} > \text{LCST}$ ) under constant and vigorous stirring. Under these conditions, the solution becomes cloudy, consisting of dispersed powder chunks. The so-formed “complete dispersion” of the CE powder, was subsequently cooled to room temperature (below the LCST) with continued gentle stirring for at least 24 h until getting a transparent (indicating a good dissolution of the chunks), homogeneous solution. CE solutions with  $10 \times 10^{-3}$ ,  $15 \times 10^{-3}$ , and  $20 \times 10^{-3}$  mol/L sodium dodecyl sulfate (SDS) were prepared by adding SDS at room temperature under stirring in one of the above described solutions. The new solution was kept under gentle stirring for at least 12 h in order to achieve complete dissolution of the surfactant.

The surface tension of the 0.34% wt CE solution was measured using the pendant drop method<sup>11</sup> (ITC Concept, Tracker), through the shape of the drop fitted to the Laplace equation. We found a value of about  $40 \pm 3 \text{ mN m}^{-1}$  at  $20^\circ\text{C}$ . Its contact angle on an untreated microscope glass plate was measured directly using an image processing system. A  $20\text{-}\mu\text{L}$  drop was deposited on the top of a flat glass plate rigorously cleaned (with ethanol, acetone, and distilled water) and the contact angles was measured on the picture. We found a value around  $35^\circ$ , which means a relatively good wetting.

For some tests, a commercial sunflower oil from Carrefour (France) was used, of density equal to  $0.92 \text{ g cm}^{-3}$  and surface tension around  $31 \text{ mN m}^{-1}$ . The contact angle of this fluid with the beads was close to 0 (clearly better wetting properties compared to the CE solution above).

### Rheometry

**Flow Curves.** Flow curve (stress or viscosity vs. shear rate in steady state) measurements were carried out at room temperature ( $20\text{--}22^\circ\text{C}$ ) with a Bohlin C-VOR (Malvern Instruments, UK) stress-controlled rheometer equipped with a stainless steel cone/plate ( $4^\circ/40 \text{ mm}$  diameter) geometry, with the plate covered with sandpaper (this reduces the risk of wall slip but it was anyway checked from experiments with rough or smooth parallel disks geometry that wall slip was negligible). After applying preshear stress (ranging from 3 Pa for the 0.17 wt % CE solution to 50 Pa for the 1 wt % solution) for 10 s, followed by a few seconds at rest, an increasing-decreasing stress ramp was imposed. We observed that the increasing curve is very close to the decreasing curve. This means that our materials are not thixotropic, a not unexpected result for a polymer solution, even if it may form aggregates. In some cases (especially at low concentrations), there was a slight discrepancy between the two curves, a discrepancy that we can attribute to a slight evolution of the shape of the free surface at the periphery. In the following, we focus on the increasing curve only and consider it as the flow curve of the material.

Our results show that the CE solutions do not exhibit a yield stress. They exhibit a constant viscosity at low shear rates and a shear-thinning behavior at high shear rates, but the critical shear rate at which the transition between these two regimes occurs decreases when the concentration increases (see Figure 1). As expected, the apparent viscosity of the solution increases with the CE concentration. Note that the behavior of the 0.34% CE solution is similar to that of the Newtonian oil at low shear rates (below  $30 \text{ s}^{-1}$ ; see Figure 1).

**Linear Viscoelastic Moduli.** Dynamic storage ( $G'$ ) and loss modulus ( $G''$ ) measurements were performed at  $20^\circ\text{C}$  with a Physica 501 (Anton Paar, Austria) rheometer equipped with a 8 mm diameter stainless steel plate/plate geometry. First, we performed a dynamic strain sweep at a constant angular frequency  $\omega$  (here  $1 \text{ rad s}^{-1}$ ) with varying the strain amplitude  $\gamma$ , to establish the regime of linear viscoelastic response for the set frequency. Then, a dynamic time sweep at a given frequency and strain amplitude in the linear regime confirmed the steady-state measurements (i.e., equilibrium conditions), consistent with the flow curves of Figure 1. Finally, we performed a dynamic frequency sweep (DFS) by setting a constant strain amplitude in the linear regime and varying the imposed frequency. The probed frequency spectrum, that is, the frequency-dependent  $G'$  and  $G''$  provided a fingerprinting of the material's relaxation dynamics.

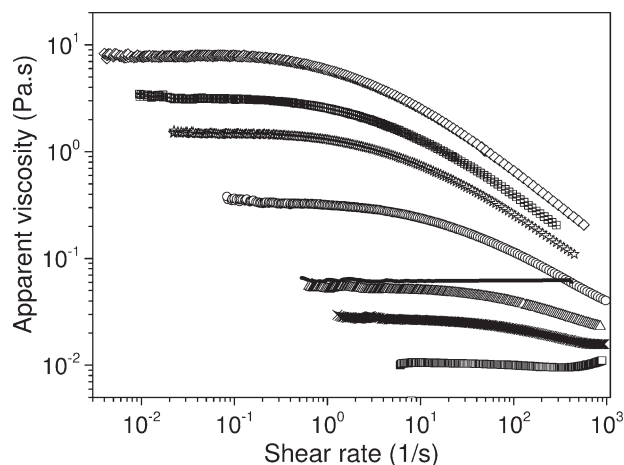


**Figure 1. Apparent viscosity as a function of shear rate for CE solutions at different wt concentrations (from lowest curve to the right, to the highest curve to the left): 0.17%, 0.25%, 0.34%, 0.5%, 0.68%, 0.8%, 1%.**

The thick continuous line corresponds to the oil.

### Bead packing

Bead packings were made by simply hand packing glass beads. Glass beads were purchased from CVP Abrasif & Broyage (France) with two different ranges of diameters: 45–90  $\mu\text{m}$  (small beads) and 150–250  $\mu\text{m}$  (large beads). These glass beads were used without specific cleaning or fractionation in size. For each one, the grain size distribution was essentially in the form of a curve in a narrow range with a peak around a mean value (a characteristic length), and after rescaling it by this mean value the different curves fall along a master curve.<sup>12</sup> As a consequence, we will assume that each can be described by a single bead diameter (i.e., this mean value,  $D$ ) equal either to 65 and 200  $\mu\text{m}$ , respectively, which plays the role of this characteristic length.

### Soaking experimental setup

The liquid was initially poured over the porous medium (i.e., the sample), then it progressively flowed through it. The sample is simply lying at the bottom of a larger container so that when the liquid arrives at the sample bottom it starts to fill the container (see Figure 2). This set-up is put in the center of the magnet of our magnetic resonance imaging (MRI) machine which makes it possible to follow the liquid distribution in the sample in time.

### MRI technique

**Spectrometer.** The Nuclear Magnetic Resonance (NMR) studies were performed on a vertical imaging spectrometer DBX 24/80 Bruker operating at 0.5T (20 MHz proton), and equipped with a birdcage radio frequency coil 20 cm inner diameter and with gradient power of 50 mT m<sup>-1</sup>.

**Profiles Acquisition Method.** The NMR profiles of water content were obtained with a double spin echo sequence<sup>13</sup>

$$\frac{\pi}{2} - \frac{t_e}{2} - \pi - \frac{t_e}{2} - S_1 - \frac{t_e}{2} - \pi - \frac{t_e}{2} - S_2 - t_R$$

where  $\frac{\pi}{2}$  and  $\pi$  are hard pulses,  $t_e$  is echo time,  $S_1$  is the first signal measured and  $S_2$  the second one, and  $t_R$  the repetition delay. Since as a first approximation the NMR signal in CE solution and in porous media plus solution is mono-

exponential, an exponential extrapolation is possible ( $S_0 = S_1^2/S_2$ ) and give  $S_0$  without relaxation.

For CE solutions, the NMR relaxation time  $T_1$  is close to 2.4 s, like bulk water in such a magnetic field, but when mixed with glass beads  $T_1$  is  $\sim 150$ –400 ms depending on bead size. The repetition time  $t_R$  is generally fixed at  $5T_1$ . For the CE solution in beads, a  $t_R$  of 3 s is thus sufficient, allowing a measurement time  $t_{\text{exp}}$  of 30 s, but for the CE solution alone (i.e., situated outside the bead packing) a  $t_R$  of 12 s would be necessary to get all the signal, which would lead to much longer times for each measurement. So, we have taken  $t_R = 3$  s to have the shortest profile acquisition. The consequence is a straightforward measurement for beads and  $T_1$  weighting for CE solution that is corrected afterward. The other parameters are  $t_e$ : 7.25 ms, the field of view (FoV): 20 cm, Matrix: 512, so that the profile resolution is 0.4 mm.

**Profile Normalization.** To obtain a saturation profile, a reference is done with a sample of water in the same Plexiglas tube, and with the same parameters, except for  $t_R = 13$  s. The profiles  $S_0$  obtained for experiments with CE solution and glass beads were directly divided by this reference profile  $S_0$ . There are two advantages to use this method: to correct the slight homogeneity default at the edge of the NMR probe and to obtain directly profiles of the saturation in porous material, that is, the distribution along the vertical sample axis of the liquid to void volume ratio.

**Image Acquisition.** The NMR images were obtained with classical method of spin echo sequence. Two kinds of images were analyzed: along vertical and horizontal axis. The sequences parameters for vertical images are: RD: 400 ms,  $t_e$ : 7 ms, matrix:  $128 \times 64$ , FoV:  $20 \times 10$  cm, 7–10 slices of thickness: 6 mm,  $N_{\text{acq}}$ : 32,  $t_{\text{exp}}$ : 14 min, and for horizontal images: FoV:  $10 \times 10$  cm, 12 slices of thickness: 7 mm.

### Theoretical considerations

Let us assume that a Newtonian liquid (of viscosity  $\eta$ ) flows in direction  $z$  through the porous medium in the form of a homogeneous transversal front progressing at the velocity  $u$  (see Figure 2). The porous medium is thus saturated (voids filled with water) up to the depth  $h$  and dry elsewhere. The height of fluid above the medium is noted  $h_0$ . We can apply the Darcy's law to this flow,<sup>12,14</sup> that is,  $u = dh/dt = (K/\mu)\nabla(p + \rho gz)$  where  $p$  is the pressure. At the front, the pressure is equal to the ambient pressure minus the Laplace pressure, which may be written  $\sigma \cos \theta / \alpha R$ , in which  $R$  is the particle

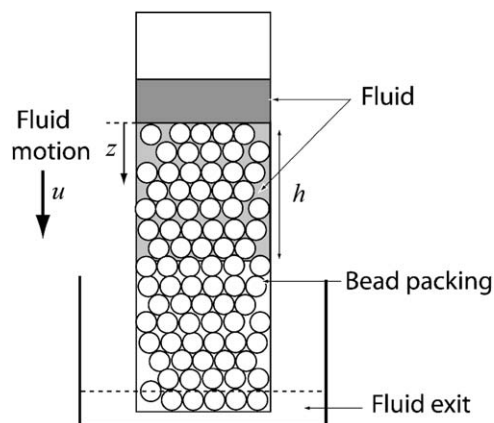


**Figure 2. Schematic illustration of the experimental setup for the soaking experiments.**



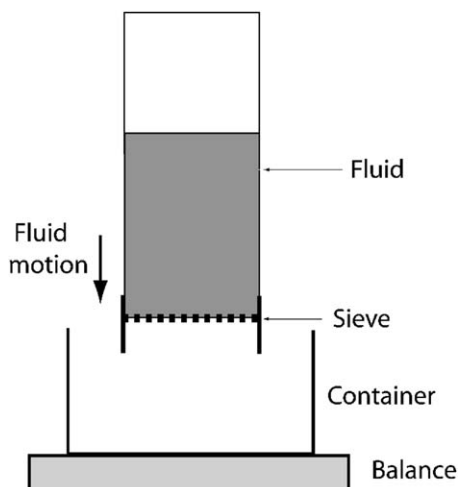


**Figure 3. Schematic illustration of the assembly used for the filtration tests.**

radius,  $\sigma$  the surface tension, and  $\theta$  the contact angle. This expression assumes an average curvature of the meniscus along the liquid-air interface at the front proportional to the bead curvature ( $1/R$ ) by a factor  $\alpha$ .

Finally, we deduce

$$\frac{dh}{dt} = \frac{K \rho g (h+h_0) + \sigma \cos \theta / r}{\eta h} \quad (1)$$

From the conservation of mass we have:  $H_0 S = h_0 S + h \varepsilon S$ , in which  $S$  is the section area of the sample and  $\varepsilon$  the porosity of the sample. Equation 1 may be rewritten as  $dh/Bdt = (A+h)/h$  whose solution is

$$h - A \ln(1+h/A) = Bt \quad (2)$$

With  $A = (H_0 + \sigma \cos \theta / \alpha \rho g R) / (1 - \varepsilon)$  and  $B = K \rho g (1 - \varepsilon) / \eta$ . The Washburn imbibition<sup>15</sup> equation is written for negligible gravity effects ( $\alpha R \rho g (h+h_0) / \sigma \cos \theta \ll 1$ )

$$h^2 \approx 2ABt \approx 2\sigma K t \cos \theta / \alpha R \eta \quad (3)$$

For similar porous media except for their characteristic length ( $D$ ), we deduce from scaling arguments that the permeability should be proportional to  $D^2$ :  $K = \beta D^2$ . It was shown<sup>12</sup> that for such materials the scaling constant  $\beta$  is around  $7 \times 10^{-4}$ . Conversely,  $\alpha$  is related to the size of the typical meniscus with regards to the particle radius, we expect it to be of the order of  $1/5$ . Under these conditions, for the oil and the 0.34% CE solution (which have very close values of the product  $\sigma \cos \theta$ , that is, about 33 mPa m for the CE and 31 mPa m for the oil) Eq. 3 reduces to

$$h \approx 0.15 \sqrt{t} \quad (4)$$

with  $h$  expressed in centimeters.

### Filtration experiments

For these tests, a plexiglass tube (70 mm inner diameter and 24 cm long) closed at its lower end by a sieve with metal cloth sieving was vertically fixed above a container (see Figure 3). A ruler was fixed on the outside of the column. We blocked the end of the tube with a solid foam plug inserted under the sieve in order to maintain the fluid in the column while filling it. We poured the fluid into the tube along the inner surface of the column to reduce bubble formation. Then, at the initial

time we removed the plug and let the fluid flow freely through the sieve. The fluid that fell in the container was recorded in time. We tested different sieve mesh widths ranging from 20 to 160  $\mu\text{m}$  and different initial heights of fluid (5, 10, and 20 cm).

We estimate the fluid flows through the sieve during the filtration test via the mass of water which passes through the sieve over some duration. We thus define the fraction of fluid outlet ( $1 - \text{WR}$ ) as  $m_{\text{outlet}}/m_0$ , where  $m_0$  is the total mass of water added above the sieve.

### Structural characterization techniques

**Grain Size Distribution Measurements for CE Solutions.** Particle diameter and polydispersity were measured with a laser diffraction particle-size analyzer (Mastersizer 2000, Malvern, UK) using the Mie diffraction theory<sup>16</sup> (coupling diffraction and diffusion). The analysis was done assuming that the particles are spherical and described by a complex refractive index. It is worth mentioning that for CE, given their variety of shapes, this type of particle-size analysis only provides information about an apparent size distribution. We discuss further this problem below.

**Centrifugation and Recuperation Cycles.** Our centrifugation-recuperation cycles consist in centrifuging a 0.34% wt MH100000 solution at 3500 rpm for 5 min twice and a third time for 10 min. After each centrifugation, we withdraw the fluid from the bottom of the tube and centrifuge again the supernatant. In this way, with the successive centrifugations and given that the sedimentation speed is linked to the particle radius, we were able to separate the big elements from the small ones, hence more centrifugation cycles *a priori* lead to smaller objects in the final suspension.

In the end, we could analyze each tube fluid batch from the tube bottom (containing the biggest elements) with microscopy and rheometry, while the respective supernatant (containing the smallest elements) could be analyzed by dynamic light scattering (DLS).

**Optical Microscopy.** We used a Leica DM-RM microscope interfaced with a DFW-V500 CCD camera (Leica Microsystems, Germany). It was equipped with two polarizing filters, that is, polarizer and analyzer, which enabled the visualization of crystalline materials which are birefringent, as some of the present CE solutions discussed below.

**Dynamic Light Scattering.** DLS was performed with a ALV-5000 (from ALV GmbH Langen, Germany) setup involving a goniometer and thermostatically controlled sample holding area. A continuum wave Nd:Yag laser from Torus, with a maximum output power of 130 mW, operating at a wavelength of  $\lambda = 532$  nm. The time autocorrelation function of the scattered intensity  $G(q, t)$  determined with the aid of an ALV-5000/E fast multi- $\tau$  correlator in the time range  $10^{-7} - 10^3$  s. Here  $q = 4\pi n / \lambda \cdot \sin(\theta/2)$  is the scattering vector and  $\theta$  the scattering angle. The measurement consisted of obtaining the intermediate scattering (field) function  $C(q, t) = [(G(q, t) - 1)/f_*]^{1/2}$  in the polarized (VV) geometry (incident and scattered beam perpendicularly polarized with respect to the scattering plane), where  $f_*$  is an instrumental factor relating to the coherence area.<sup>17</sup> This function was analyzed with a Laplace inversion program appropriate for polydisperse systems (CONTIN).<sup>18</sup> The decay rate,  $\Gamma$ , is related to the diffusion coefficient,  $D$ , as  $\Gamma = D \cdot q^2$ . For translational diffusion, the hydrodynamic radius of the suspended

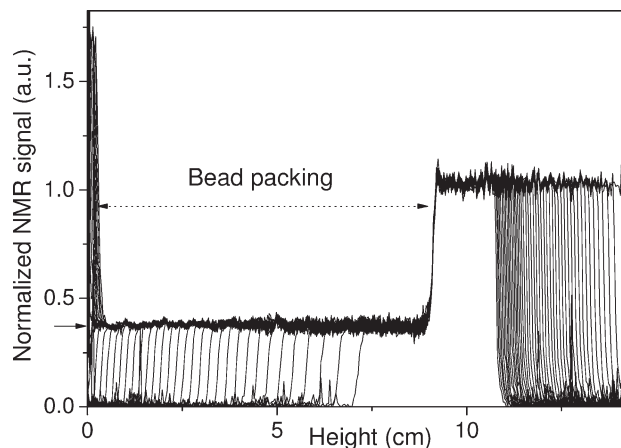


**Figure 4. Typical experimental results for the flow of oil through a bead packing (large beads).**

Successive water distribution profile in time (from right to left) every 5 min (except for the initial one).

elements,  $R_h$ , can be calculated using the Stokes–Einstein–Sutherland equation

$$R_h = \frac{k_B T}{6\pi\eta_s D} \quad (5)$$

where  $k_B$  is the Boltzmann constant and  $T$  is the absolute temperature.

Prior to DLS measurements, all samples were prepared as discussed in section *Materials* with ultrapure milli-Q water, equilibrated overnight at room temperature and filtered through cellulose mixture filters of 0.8  $\mu\text{m}$  pore size. The DLS analysis aimed at elucidating the changing dynamic structure and interactions of the CE solutions during centrifugation and filtration cycles as discussed in above sections. The following protocol was used during measurements: first, the 0.34% wt solution was centrifuged three times at room temperature and 2 mL of the final supernatant solution were taken. This solution was subsequently filtered through 0.8  $\mu\text{m}$  cellulose mix filter for aqueous solutions. The temperature was stabilized at 20°C and the DLS experiment was performed. Selective higher temperature measurements were performed by heating the sample to 50°C and equilibrating it for 30 min.

## Experimental Results and Discussion

### Flow of Newtonian fluid through porous bed

A typical series of successive density profiles in time for the test with oil is shown in Figure 4.

Initially, all the liquid is above the sample, but later it starts flowing through the sample during the measurement in the MRI magnet. In other words, the liquid progressively invades the porous medium. The apparent density of liquid is given from the normalized NMR signal, which is equal to the ratio of the NMR signal to that measured in a region of liquid alone (i.e., above the sample). Here, this apparent density is around 37% (see small arrow in Figure 4) in the wetted region inside the sample (see Figure 4), which is the typical porosity of a granular packing of almost uniform beads. We deduce that the voids inside the sample are entirely filled with water. As a consequence, the porous medium is saturated up to the air-liquid interface, that is, the front, which is associated with the step progressing from right to left with time in Figure 4. More-

over, the front is almost straight (almost vertical density profile) which means that negligible fingering effect occurs at the front, otherwise we would have partially saturated region around the front visible as a decrease of the apparent density below 37%. The front advances but its velocity progressively decreases as may be seen from the reduced distance between two successive fronts in Figure 4. Finally, it reaches the sample bottom and the liquid enters the container, leading to an apparent liquid density in the profiles at the bottom larger than 1 because the container cross-section area is larger than that of the porous sample. The homogeneity of the fluid distribution in the sample was confirmed by a series of two-dimensional MRI pictures which show that the sample appears saturated in the wetted regions identified in the density profiles.

We could follow the advance of the liquid front by measuring its position on the density profile. A more precise technique consists in integrating the part of density profile inside the bead packing, and following it in time. This directly provides the average position of the equivalent flat front progressing through the sample. We checked that computing the loss of liquid above the sample by integrating the part of density profile situated above provides the same result, which proves the consistency of our approach and again confirms that the sample is saturated up to the front.

We can see that the front position varies essentially with a slope  $1/2$  as a function of time in a logarithmic scale (see Figure 5), which corresponds to a typical Washburn process (cf. Eq. 4). However, when the depth of penetration is large (say, more than about 5 cm) the data slightly depart from this simple behavior because the additional gravity terms (see above) are no longer negligible, but it is out of the scope of this article to study further this point. Finally, the Washburn equation fitted to these data at sufficiently small depths in the form  $h = k\sqrt{t}$  has a coefficient  $k = 0.16$ , very close to the value (0.15) found in the theoretical considerations (see Eq. 4), which confirms our physical analysis of the process.

### Flow of CE solutions through porous bed

For the CE solutions, the results are different. At the beginning, the penetration seems similar to that for oil: a nearly

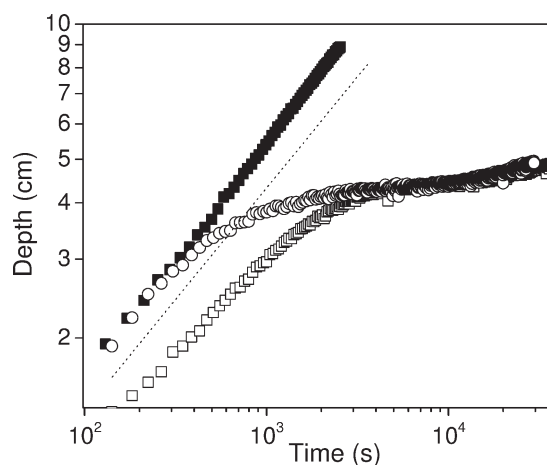


**Figure 5. Experimental results for the flow of oil (filled squares) through large beads or 0.34% wt CE solution through large beads (circles) or small beads (squares): apparent depth of penetration as a function of time.**

The dotted line of slope  $1/2$  is a guide for the eye.

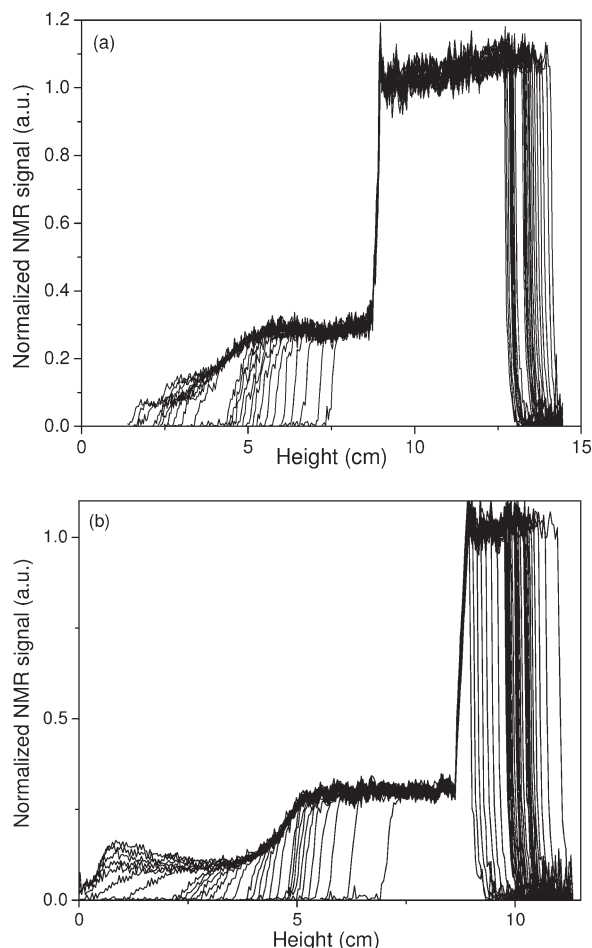


**Figure 6. (a) Experimental results for the flow of a CE solution (0.34% wt) through a bead packing (small size). Successive density profiles in time (from right to left): every 2 min for the first 15 profiles, then every 30 min for the next seven profiles and every 2 h for the last three ones. (b) Experimental results for the flow of a 0.34% wt CE solution through a bead packing (large size). Successive density profiles (from right to left): every 90 s for the first 10 profiles, every 15 min for the next 6 profiles, every 1 h for the next 8 profiles, every 10 h for the next 7 profiles.**

straight front enters rapidly through the bead packing. Then, there is a slowing down of the advance followed by a partial saturation in the advance (see Figures 6a, b). Looking at the MRI pictures in cross-sections at the end of the test, we note that the region of partial saturation is in fact associated with a heterogeneous distribution of liquid at the scale of the sample, as we can see regions of very different liquid content (see Figures 7 and 8). This should reflect a heterogeneous structure of the CE solution and will be further discussed below.

We can again follow the penetration depth of an equivalent homogeneous front progressively saturating the sample, by integrating the density profiles in the liquid part above the sample. Even if we know that this is not physically realistic when the saturation becomes heterogeneous, this represents nevertheless the average mass of solution penetrating the sample in time. For the particular CE solution (0.34% wt) flowing through large beads, we can see that the advance of the front

in the first period is the same as for the oil of same viscosity (see Figure 5), the soaking process is well described by the Washburn equation (4) with a coefficient  $k$  again very close to that predicted by theory. Then, the curve for the CE solution strongly departs from that for the oil, which reflects a significant slowing-down of the advance front. Actually, the curve tends to reach a plateau (see Figure 5). This suggests that at the beginning the solution essentially behaves as a simple liquid but after some time of flow there appears to be some kind of jamming of the CE solution in the pores, which again reflects its structural heterogeneity and will be discussed below.

The advance of the same solution through the small beads is also consistent with the Washburn process (see Figure 5). The coefficient of Eq. 4 is now 0.1, close to the value predicted by the theory, considering that it is simply equal to the coefficient for the large beads times the square root of the bead radius ratio which gives 0.09. Then, the curve reaches the same apparent plateau as for the large beads. This means that the jamming occurs for the same amount of CE in the porous medium.

The results are qualitatively similar for a more concentrated CE solution (0.68% wt), that is, Washburn imbibition during a first period followed by a plateau (see Figure 9). The slope of the equation is now 0.037 for the large beads. Given that the viscosity of this solution is about 25 times that of the 0.34% wt CE solution (at low shear rates, which correspond to those encountered in the porous medium), we would expect a theoretical coefficient of  $k = 0.032$ , in good agreement with the experimental findings. A slightly larger discrepancy exists

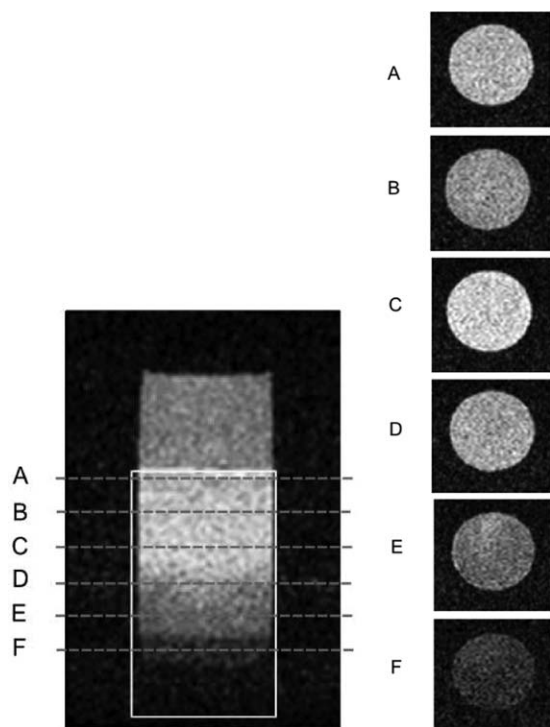


**Figure 7. (Left) Location of the cross-sections in a longitudinal density image of the sample. The yellow frame indicates the boundaries of the sample. (Right) Density images in cross-sections at different levels in the sample (bead packing) for the test described in Figure 6a.**



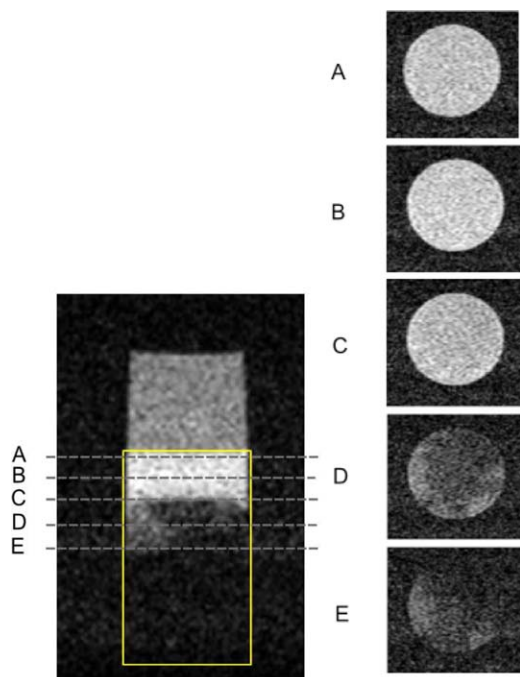


**Figure 8.** (Left) Location of the cross-sections in a longitudinal density image of the sample. The yellow frame indicates the boundaries of the sample. (Right) Density images in cross-sections at different levels in the sample (bead packing) for the test described in Figure 6b.

[Color figure can be viewed in the online issue, which is available at [wileyonlinelibrary.com](http://wileyonlinelibrary.com).]

with the data at small bead radius as the experimental coefficient is 0.03 whereas the theory predicts 0.018. Globally, the experimental results nevertheless are consistent with the theoretical predictions and we have no explanation for these specific discrepancies.

For the 0.68% wt CE solutions, the plateau levels for the large and small beads are slightly different but the most interesting point is that in those cases we have information over very long times. Thus, it is possible to observe that after some time the plateau ends with a new increase of the equivalent length in time, which exhibits again a slope  $1/2$  as for the Washburn process. If we compare the position of this curve to that for the initial period, we conclude that all occurs as if the liquid was now flowing through a new porous medium of lower permeability. This analysis is confirmed by the fact that the two curves (although we do not have data over very long times for the larger particles) seem to be similar in this period: the liquid flows through an effective new porous media which has been created by the jamming of the same CE solution in the bead packing. In this context, it is natural to assume that this is now essentially water which flows through a polymer matrix jammed in the solid structure.

From the position of the curve over long times, we now find a coefficient of Eq. 4 equal to 0.008. Using the viscosity and surface tension of water, we infer that if this new porous network could be considered as a bead packing the radius of the beads should be  $1/600$  times smaller than the effective bead packing length, that is a diameter of about  $0.1 \mu\text{m}$ .

In summary, the picture we finally get from these data is as follows: the CE solution first penetrates like a simple liquid,

then a progressive jamming occurs rapidly leading to its almost complete stoppage, finally the water can slowly flow through a new very thin porous medium created by the jamming of CE.

Such results show that in contrast to simple Newtonian liquids (like oil), for a non-Newtonian liquid a jamming of the elements in the porous sample occurs. Such an effect could *a priori* not occur if the solution were fully homogeneous at molecular level, that is, only made of isolated chains able to molecularly disperse. In that case, we would expect to see an imbibition governed by the apparent viscosity of the suspension. Hence, there is a need to further characterize these CE solutions in order to understand this jamming effect and its connection to the flow through bead beds.

### Characterization of CE solutions

*Characterization of Suspended CE Elements via Laser Particle Sizing.* The results of a laser particle sizing of a 0.34% wt CE solution are shown in Figure 10. The data show a high polydispersity of the objects in suspension, from  $5$  to  $500 \mu\text{m}$ , with two peaks around  $80$  and  $200 \mu\text{m}$ . Note that we do not mention solution but suspension instead as there is evidence of big cluster formation even in this concentration which is estimated to be about of  $c^*/3$ , in which  $c^*$  is the coil overlap concentration marking the onset of semidilute regime:  $c^* = 3M_w/4\pi R^3 N_A$  with  $M_w$  the molar mass,  $R$  the coil radius, and  $N_A$  the Avogadro number. It is worth mentioning that the method used here for the calculation of particle sizing makes the assumption of spherical solid particles, which is not exact in our case: thus, it cannot give us an exact particle size but a range of apparent particle sizes. However, such data tend to confirm the presence of a significant volume fraction of very large size elements in suspension in the liquid.

At this point, it is useful to attempt at estimating the size of the single CE molecule. This can only be approximate as it is known that, despite their widespread use in numerous applications and their characterization reported in the literature, cellulosic polymers are still not well understood in terms of structure and solution properties.<sup>19–22</sup> In very broad terms, one

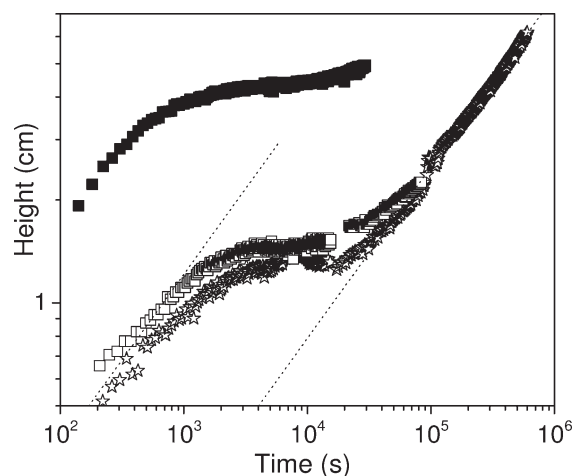


**Figure 9.** Experimental results for the flow of 0.34% wt CE solution through large beads (filled squares) or 0.68% wt CE solution through large beads (open squares) or small beads (stars): apparent depth of penetration as a function of time.

The dotted lines of slope  $1/2$  are guide for the eye.

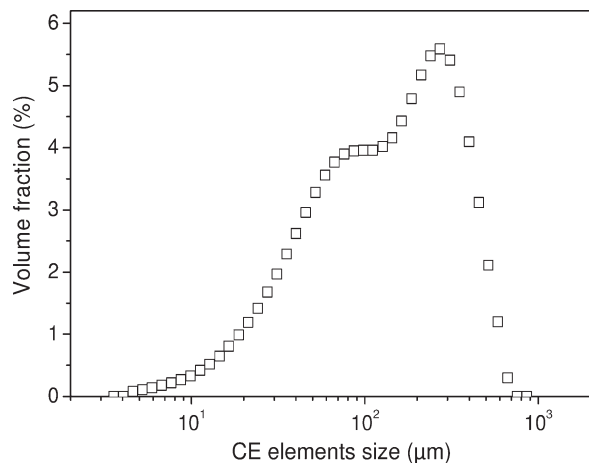


**Figure 10.** Particle size distribution for a 0.34% wt CE solution.

can say that, given the variety of grades available, cellulosic ethers can be flexible or semiflexible chains, with nearly always high molar mass. Usually, they dissolve in water at room temperature, albeit not easily, but exhibit LCST behavior, that is, they phase separate upon heating, as already discussed. It has also been reported that they may crystallize and/or form gel networks or large aggregates.<sup>19–21,23</sup> To obtain a reasonable, albeit rough estimate of the molecular size of the present CE in water, we consider it to be a flexible long polymer with average molar mass  $M_w = 10^6 \text{ g mol}^{-1}$  (based on an apparent zero-shear viscosity of 100 Pa s in 2% wt aqueous solution).<sup>2,10,22</sup> With water being a nearly ideal solvent at room temperature,<sup>5</sup> the average end-to-end distance  $\langle R \rangle = b\sqrt{C_\infty N}$  where  $N$  is the degree of polymerization,<sup>4</sup>  $C_\infty$  Flory's characteristic ratio (here taken about 3<sup>24</sup>) and  $b$  the monomer length (roughly taken as 0.6 nm<sup>24</sup>). With the monomer molar mass being  $M_0 = 588 \text{ g mol}^{-1}$  we get  $N = 1700$ , hence  $\langle R \rangle \approx 43 \text{ nm}$ . The respective radius of gyration<sup>4</sup> is  $R_g = \langle R \rangle / \sqrt{6} = 18 \text{ nm}$ . Given the approximate nature of the approach, this value is reasonably consistent with the prediction of an empirical law<sup>5</sup> which relates the radius of gyration to the molar mass:  $R_g = K_{R_g} M_w^v$ , with  $K_{R_g} = 3.8 \times 10^{-2} \text{ nm}$  and  $v = 0.53$ , for CE molecules similar to our polymers (hydroxymethylcellulose).<sup>4,19</sup> So far, we assumed that CE dissolves in water without problems. Note that from the above numbers, the extracted overlap concentration is  $c^* \approx 1\% \text{ wt}$ .

To complete the molecular characterization of the sample, we run a gel permeation chromatography (GPC) test with tylose samples dissolved in water/phosphate buffer and subsequently filtered. We found that the polymer is highly polydisperse, with a polydispersity index (weight-to-number average molar mass ratio)  $M_w/M_n \approx 8$ , and  $M_w \approx 550,000 \text{ g/mol}$ , confirming the above results and choice of molar mass for analysis.

**Optical Microscopy of Suspended CE Elements.** Microscopy observations of the 0.34% wt solution tend to confirm that it contains elements of complex nonspherical shapes and typical apparent size of the order of 100  $\mu\text{m}$ , but a significant fraction of smaller elements, not detectable, could also exist.

To have a better view of the size and structure of these elements a natural idea is to separate them by size. In this spirit, we performed successive centrifugation-recuperation cycles (following a procedure similar to the filtration tests discussed below) and after each centrifugation we analyzed the bottom of the tubes, which contains the largest elements, by microscopy, and the supernatant, which contains the smallest elements, by DLS.

Polarized optical microscopy images of the bottom fluid, that is, sediment (see Figure 11) show that the CE elements present after the first centrifugation are bigger (from 100 to a few hundred microns) than those present after the third centrifugation (which are of the order of a few tenths of microns). The bright color of the largest CE elements suggests that they exhibit a semicrystalline structure, which is not the case for the smallest elements. The large elements are also clearly anisotropic and their fibrillar-like structure conforms to recent literature reports on methylcellulose solutions,<sup>25</sup> but we note that this could be also due in part to the effect of the deposition of the clusters on the glass microscope plate. Conversely, this could be interpreted as a reflection of the cluster deformability. Clearly, the large size of polydisperse clusters of different shapes is important for the jamming phenomenon associated with the filtration experiments (see Section *Filtration tests*).

**DLS Analysis of Suspended CE Elements.** We now look at the dynamics of the supernatant solution after the third centrifugation (see Section *Dynamic Light Scattering*), at 20°C. The intermediate scattering function  $C(q, t)$  at a scattering angle of 90° (i.e., scattering wavevector  $q = 0.022 \text{ nm}^{-1}$ ) is shown in Figure 12. It reveals two distinct relaxation processes, from which we can obtain some size estimates. (1) The fast process yields a diffusive process (see insets of Figure 12 showing  $q^2$ -dependent relaxation rate and  $q$ -independent

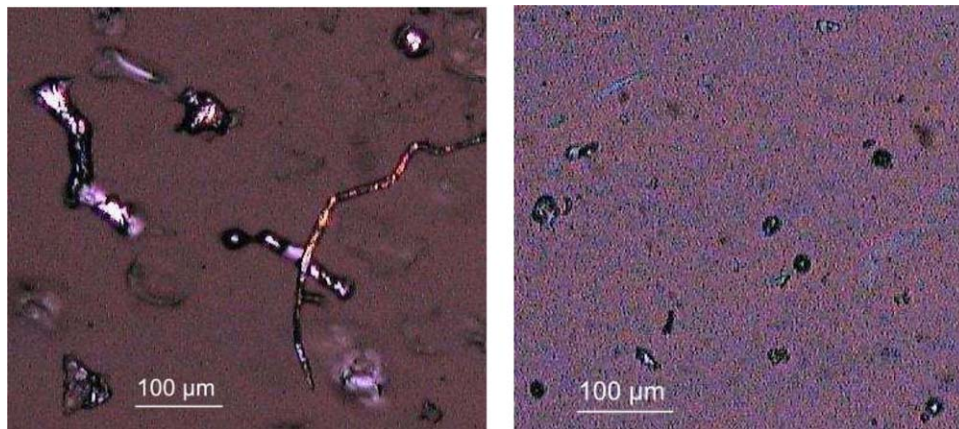


**Figure 11.** Polarized microscopy of the bottom fluid after (left) the first or (right) third centrifugation.

[Color figure can be viewed in the online issue, which is available at [wileyonlinelibrary.com](http://wileyonlinelibrary.com).]



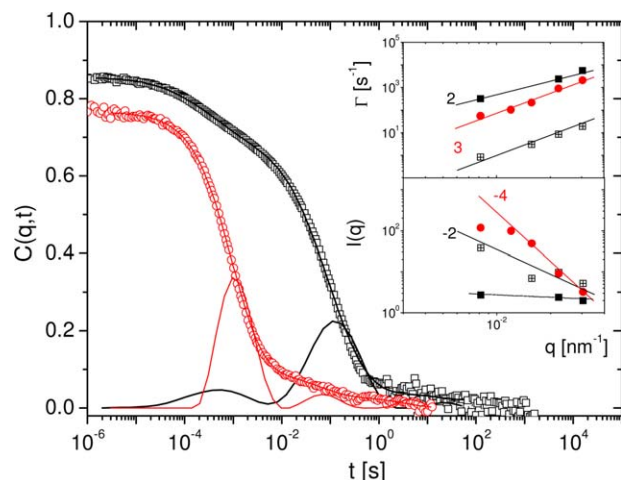


**Figure 12. Normalized intermediate DLS function  $C(q, t)$  at  $q = 0.022 \text{ nm}^{-1}$  and  $20^\circ\text{C}$ , for the supernatant of the third centrifugation of the 0.34% wt aqueous CE solution (open squares, right).**

The respective  $C(q, t)$  after diluting this solution by 5000 times is also shown (open circles, left). The solid lines represent the distribution of relaxation times via CONTIN and the respective fits to  $C(q, t)$ . Insets: The dependence of the relaxation rates of the different modes of the correlation functions (top) and their (intensities) on  $q$  (see text). The lines are drawn to guide the eye and indicate the slopes (numbers). [Color figure can be viewed in the online issue, which is available at [wileyonlinelibrary.com](http://wileyonlinelibrary.com).]

intensity) with hydrodynamic radius  $R_h = 47 \text{ nm}$  and an apparent radius of gyration  $R_g = 38 \text{ nm}$ , which relates to some sort of sphere-like objects (note that  $R_h/R_g \approx 1.24$ , a value not far from that of hard spheres<sup>26</sup>) or interactions. (2) Conversely, the slow process is also diffusive and yields  $R_h = 19 \mu\text{m}$  with  $q^{-2}$ -dependent intensity (insets of Figure 12), suggesting long flexible structure. As we diluted the sample further (by 55 times), the slow process virtually disappeared and  $C(q, t)$  relaxed essentially via one process with  $q^{-2}$ -dependent intensity and  $R_h \approx 250 \text{ nm}$ , that is, slower than the fast process but faster than the slow process of the first concentration (data not shown). At the next dilution (5000 times the original),  $C(q, t)$  is still composed of one dominant process, but with stronger  $q$ -dependence of both rate and intensity (Figure 12). Analysis yields an apparent  $R_h = 260 \text{ nm}$ . Hence, large polydisperse structures persist at this level of dilution as well. We diluted further (500,000 times) and observed features and estimated similar size as in the 5000 case (data not shown). We note that these measurements only provide a qualitative (albeit consistent) picture and estimates as the intensity did not reach plateau at low  $q$ 's (and we still "see" inside the structure with  $qR > 1$ ) and the solvent viscosity (instead of solution viscosity) was used. It is also fair to conclude that using the specific protocol here, it was impossible to molecularly disperse the present CE in water, corroborating literature reports.<sup>19,20,27</sup> Furthermore, at any dilution, the solutions were not stable as over long time (typically 3 days) DLS revealed further aggregation. Selective measurements at  $50^\circ\text{C}$  did not provide new insights due to the competition of enhanced mobility and tendency to phase separate (above LCST) which was responsible for increased fluctuations in intensity (data not shown). Hence, the overall picture is that of a heterogeneous solution comprising of polydisperse

large clusters.<sup>19–21,23</sup> This conforms to the outcome from the filtration experiments (see Section *Filtration tests*), suggesting jamming.

Since it is now clear that clusters are formed, let us do a simple hypothesis: suppose that the CE elements are suspended in a solvent (water) of viscosity  $\eta_s$  forming virtually compact spheres (the clusters). For simplicity, let us now forget about their size polydispersity (as shown in the DLS data) and consider the viscosity of the suspension. In that case, the suspension viscosity may be estimated from the Krieger–Dougherty equation,<sup>28</sup> that is,  $\eta = \eta_s(1 - \phi/\phi_m)^{-2.5\phi_m}$ , where  $\phi$  is the volume fraction of CE particles and  $\phi_m \approx 0.64$  their maximum packing fraction (as in hard sphere colloids). We measured the viscosity of a 0.34% wt CE suspension and found a value of approximately 70 mPa s, hence we deduce  $\phi \approx 0.6$ , which means that these effective CE particles are rather close to each other. We can relate the volume fraction to the size and molar mass of the polymer in the particle,  $\phi = 4\pi R_h^3 n/3$ , with  $n$  being the number of chains per unit volume, that is,  $n = cN_A/M_w$ . Using the value found for  $\phi \approx 0.6$  and the expression for  $R_h$ , we get  $M_w \approx 2 \times 10^{11} \text{ g mol}^{-1}$ . Such a value for the molar mass is of course unrealistic (clearly the assumptions above do not hold). The corresponding  $R_h \approx 20 \mu\text{m}$ , is also much larger than that usually found for polymer chains (by coincidence, it is almost that of the slow mode of the 0.34% wt supernatant solution, see Section *DLS analysis*). This naive analysis confirms the formation of heterogeneous polydisperse clusters when CE is suspended in water, at least with the protocol used in this work.

**Viscoelastic Properties of Suspended CE Elements.** Let us now look at the linear viscoelastic response of the sediment obtained from the bottom of the tube after the first centrifugation, which can be considered as being a concentrated suspension of the CE elements of the initial suspension. From the strain sweeps, we can observe that for small deformations the elastic storage modulus of this material (see Figure 13a) is significantly higher than the viscous loss modulus, suggesting that it is a viscoelastic solid. Beyond some critical deformation amplitude the elastic modulus starts to decrease well below the viscous modulus, indicating that the material now behaves like a liquid. The yielding which characterizes the onset of liquid-like response at a strain amplitude of about 20% could be associated to deformation and break of aggregates. The DFS data (see Figure 13b) at low strains corroborate this picture and in fact suggest that the sample (with very little water) exhibits the rheological behavior of a soft gel-like network, characterized by a low-frequency plateau, that is, moderate value of storage modulus. This value of the modulus of this gel is similar to those of colloidal glasses and some colloidal

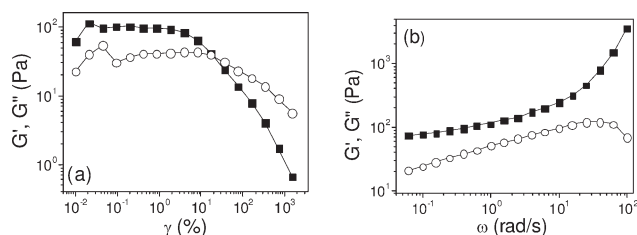


**Figure 13. Storage ( $G'$ , squares) and loss ( $G''$ , circles) moduli as a function of strain amplitude  $\gamma$  (a) and angular frequency  $\omega$  (b) for the sediment of the 0.34% wt CE solution tube after the first centrifugation.**

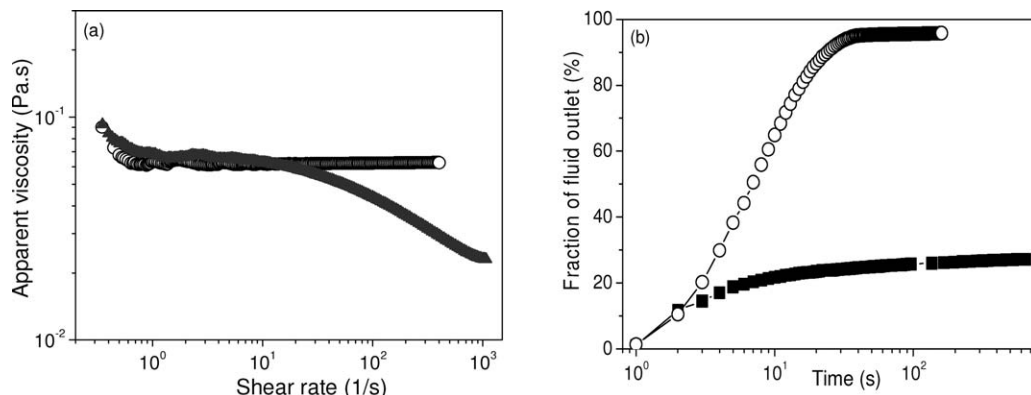


**Figure 14. (a) Apparent viscosity of the oil (empty circles), and a 0.34% wt MH100000 CE solution (filled triangles). (b) Fraction of fluid outlet 1 – WR for oil (circles) and a 0.34% wt CE solution (squares) through a sieve of 80  $\mu\text{m}$  mesh width and for an initial height of 10 cm.**

gels.<sup>28</sup> Its yield strain value is also consistent with that of colloidal glasses, and the yielding appears to conform to a ductile breaking.

As the rheological data point to the presence of a physical network, say here connected clusters, we can estimate its characteristic average mesh size from the plateau modulus as<sup>4</sup>

$$G' \approx \frac{k_B T}{\xi^3} \quad (6)$$

where  $k_B$  is the Boltzmann constant and  $\xi$  is the mesh size. Since in our case  $G' \approx 100$  Pa, we get  $\xi \approx 40$  nm, a value that is consistent with the value found by Arvidson.<sup>9</sup>

The analysis of the sediment shows that it is different from the supernatant, albeit in both cases CE elements are interacting. A speculative picture linking both together calls for formation of loose clusters in the dilute regime. During centrifugation, these elements come closer and associate (via some kind of interpenetration). Hence, the final sediment is a physical network where the original cluster size is not important anymore but the typical correlation length (average network mesh size) instead.

### Filtration tests

Considering the large size of suspended CE elements in these materials, we can further study them with the help of a straightforward test for the separation of large elements from the liquid in which they are suspended, namely filtration tests.

Let us start by comparing the flow of Newtonian fluid, that is oil, made of small molecules, with the flow of our CE solution (at 0.34% wt) through a sieve. Although the two fluids have similar apparent viscosities (in fact the CE solution viscosity is smaller at high shear rates; see Figure 14a) the simple liquid rapidly and entirely flows through the sieve (see Figure 14b). On the contrary, the CE solution first flows in a similar way over a short time then significantly slows down so that there is a slightly inclined plateau in the curve associated with a very slow flow (see Figure 14b). This means that all almost occurs as if a significant height of CE solution was stopped above the sieve. It is remarkable that this trend has a global similarity with that observed for the flow through a bead packing as observed by MRI (see Section *Flow of Newtonian fluid through porous medium*).

Such a result obviously suggests that there is a jamming of the suspended elements in the sieve holes, which then tends to block the flow of the solution situated above. For such a jamming to occur, one needs to have a network formation and at

least a fraction of the suspended objects with a size of the order of that of the sieve holes, that is, of the order of several tenths of microns. This result again confirms the presence of large objects in the CE solution, in agreement with DLS.

To further study this potential jamming effect, we conducted a filtration experiment in the spirit of the DLS successive dilution studies above. We only used the fluid outlet, recovered from the preceding test, as the incoming solution (without any addition of new solution). In other words, after every filtration test, we collected the solution that went through the sieve to reuse it as input for the next experiment, without adding any new solution or fluid that did not pass through the porous medium. Note that we kept the initial height of CE solution constant for every tests. The sieve was carefully cleaned after each test to avoid any effect due to the possible accumulation of CE on it. Under these conditions, it can be expected that the solution would progressively become poorer in CE as we should have removed the CE elements in a specific range of size (depending on the mesh width). Actually, the fluid outlet slowly increases with the increasing number of tests, but does not seem to reach the expected value of 100% after six sequences (see Figure 15).

There are different possible origins for this jamming. It may be due to some kind of accumulation of the CE elements which,

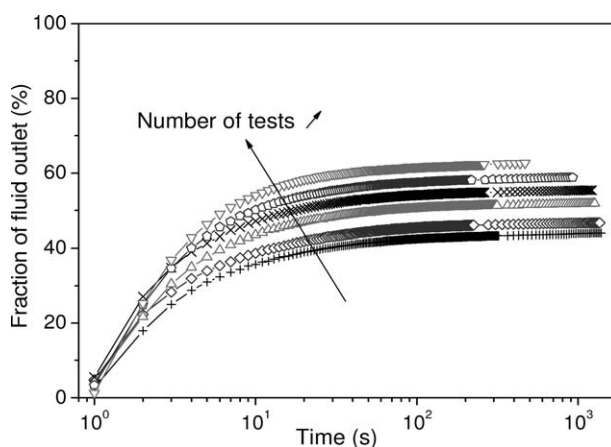


**Figure 15. Fraction of fluid outlet, 1 – WR, for successive filtration tests using only the solution outlet of the previous test for a 0.34 wt.% CE solution with a 100  $\mu\text{m}$  sieve at a initial height of 20cm.**

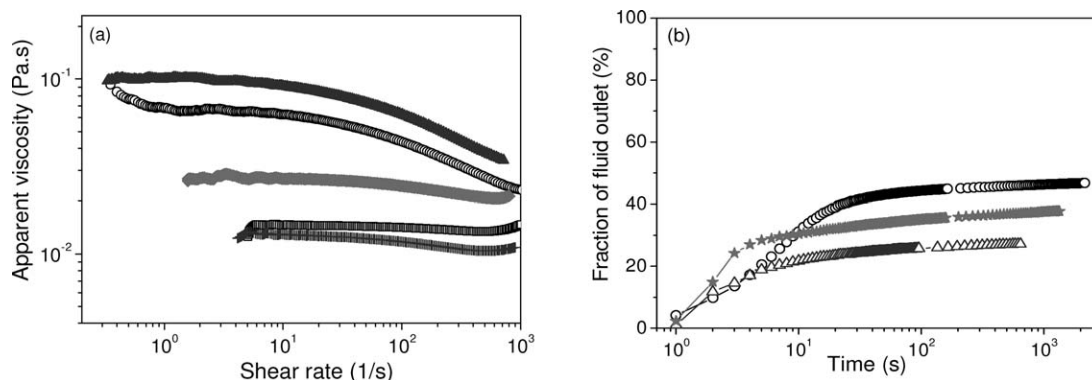


**Figure 16. (a) Impact of surfactant on a 0.34% wt CE suspension apparent viscosity: without SDS (empty circles), with 10 mmol/L SDS (filled triangles), 15 mmol/L SDS (filled diamonds), and 20 mmol/L SDS (empty squares); compared with a 0.17% wt CE suspension (plus sign). (b) Fraction of fluid outlet, 1 – WR, for 0.17% wt (filled stars) and 0.34% wt MH100000 suspensions without (empty triangles) and with 15 mmol/L SDS (empty circles) through a 80  $\mu$ m sieve and for an initial height of 10 cm.**

despite the fact that they may be smaller in size than the hole mesh, would finally clog each hole.<sup>8</sup> However, for our relatively concentrated CE suspensions the CE elements are already close to each other so that the progressive accumulation concept would not apply in the same way. There might nevertheless be a kind of collective jamming as it occurs in hopper filled with dry granular materials<sup>29</sup> when the hole to element size ratio falls below a value about 6. A last possible explanation is that the suspension contains large size elements (of the order of 100  $\mu$ m, as suggested by the laser grain sizing), which are widely deformable and thus able to jam when the pressure around the sieve hole is not sufficiently large. Such an explanation is consistent with the fact that successive filtration tests lead to almost the same result (in fact there is a slight evolution due to a slow decrease of the element concentration) and with the observation that an additional pressure applied to the top of the sample is able to unjam the flow.<sup>8</sup>

#### Impact of surfactants

We know that CE contains hydrophobic groups which, in aqueous solution would tend to group and form clusters thanks to hydrophobic interactions. To assess the strength of these associations, we studied the impact of the addition of surfactant on the flow properties of a CE solution as well as during a filtration test. The surfactant used here is SDS. Flow curves for CE suspensions with different amounts of surfactant added (all above the reference critical micelle concentration (based on pure SDS aqueous solution), cmc = 8 mmol/L) are shown in Figure 16a. This graph also shows the flow curves for the CE suspensions at 0.17 and 0.34% wt without SDS. We can see that, initially, the suspension viscosity increases slowly when adding a small amount of surfactant, then decreases slowly when the SDS concentration exceeds a certain critical value between 10 and 15 mmol/L. Moreover, we can notice that the 0.34% wt CE solution with 20 mmol/L has identical viscosity with the 0.17% wt CE solution.

This viscosity variation with the surfactant concentration could be explained by the interaction between the surfactant molecules and the CE polymer hydrophobic chains by bridging or breaking the hydrophobic associations, depending on the amount of surfactant.<sup>5</sup> We will discuss this in more detail in the next section.

Let us now look at the filtration behavior of an intermediate surfactant CE suspension with 15 mmol/L SDS and compare it

with two CE suspensions at 0.17 and 0.34% wt without SDS (see Figure 16b).

We remark that the final fraction of fluid outlet for a 0.34% wt CE suspension with SDS is significantly higher than the final fraction reached by the same suspension without surfactant (1 – WR = 45% with 15 mmol/L SDS against 1 – WR = 26% without surfactant).

Besides, it is interesting to note that the final fraction of fluid outlet of the 0.34% wt CE suspension in the presence of SDS, whose viscosity is however higher than for the 0.17% wt CE without SDS, is superior to the final fraction obtained for the latter suspension (which means that more 0.34% wt CE suspension with SDS flows through the sieve). This result highlights that the viscosity alone cannot explain the value of the plateau observed in the case of CE solution.

#### Linking the Structure of CE Solutions to Macroscopic Properties

##### *Semicrystalline structure aggregates and hydrophobic interactions*

To reconcile all experimental evidence discussed above and in particular the presence of large CE elements in water, we have to return to the microscopic structure of the CEs. CEs are synthesized from the natural cellulose which is insoluble in water due to the presence of intramolecular hydrogen bonds. During CE synthesis, some hydrophobic groups are grafted on the hydrophilic natural cellulose skeleton. These groups allow the CEs to become soluble by breaking the intramolecular hydrogen bonds and creating new hydrogen bonds between the polymer and water. However, if the number of substitutions is too high the polymer can become insoluble due to the presence of too many hydrophobic groups.<sup>19–21</sup>

During the CE synthesis, thanks to an etherification reaction the substitution of hydrophobic groups is done randomly and a small amount of unsubstituted anhydroglucose units may remain in a macromolecule. These non-substituted and insoluble segments that come from the natural cellulose will tend to cluster and form some intramolecular and intermolecular hydrogen bonds in order to decrease their interaction with the solvent.

Thereby these associations (local aggregates) can create a semicrystalline structure (due to the possible orientation of the unsubstituted units that come close) that act as an effective



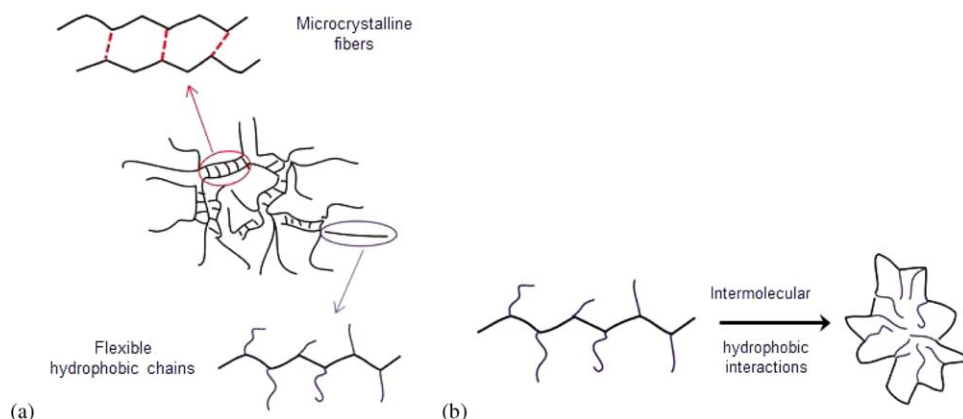


**Figure 17. (a, Left) Scheme of a star-shaped cellulose ether aggregate. The red dotted lines represent the H bonds whereas the purple curves stand for the hydrophobic chains. (b, Right) Representation of an associative polymer chain and the formation of a micelle-type flower (from Ref. 31).**

[Color figure can be viewed in the online issue, which is available at [wileyonlinelibrary.com](http://wileyonlinelibrary.com).]

cross-linker. These aggregates can be compared to a star shaped microgel, also called (aggregated fringed micelles<sup>30</sup>), where the microcrystalline fibers form the core of the structure whereas the hydrophobic branches, in contact with the solvent, have the role of flexible chains (see Figure 17a).<sup>19,20,23,25,27</sup>

It is interesting to mention that this type of association was observed in our polarized light microscopy experiments for the bottom sample obtained after the first centrifugation (larger elements) and not for the samples after the second nor the third centrifugation (see Figures 16a, b).

The second type of association results from the hydrophobic groups grafted on the hydrophilic skeleton which tend to minimize their interaction with the solvent (here water) by grouping to form aggregates<sup>31</sup> referred as “lumps,”<sup>27</sup> or “superstructures”<sup>35</sup> (see Figure 17b). This type is pure intermolecular in origin.<sup>20–23</sup> These associations would be the cause of the increase of the CE solution viscosity.<sup>27,32</sup> Unlike crystalline aggregation, these associations can break with the addition of surfactant molecules causing a reduction in viscosity.

### Addition of surfactant

The influence of adding surfactants to a CE solution has already been studied by several authors. It has been shown, as previously mentioned, that surfactants can modify CE solution rheological properties by interacting with the hydrophobic groups grafted on the CE molecules.

Therefore, when adding SDS in the CE solution, surfactant molecules will preferentially go around the polymer hydrophobic pendant chains. Depending on the surfactant concentration, with respect to the amount of hydrophobic chains, several scenarios are possible. If the surfactant concentration is low enough, hydrophobic associations will break due to the presence of the surfactant and the viscosity of the solution will decrease.<sup>5</sup> On the contrary, if the amount of surfactant in solution is increased above the reference cmc, the surfactant molecules will be able to form micelles. Note that in the complex mixture, we expect that the cmc may be smaller than the reference value of 8 mmol/L. However, if the concentration is still too low, one micelle will trap various polymer hydrophobic chains, which will induce the formation of new aggregates. In this case, the solution viscosity will increase and become larger than the initial solution without surfactant.

Finally, if the surfactant concentration is high enough and exceeds another critical value  $cmc^*$  ( $c \gg cmc^*$ ), every hydrophobic group will be surrounded by one surfactant micelle, breaking the intermolecular hydrophobic interactions and letting the polymer molecules free.<sup>33</sup> This breaking of the aggregates leads to a decrease of the solution viscosity as we observed on Figure 10 for a SDS concentration above 10 mmol/L.

This influence of surfactant on the CE aggregates structure can explain the results obtained in filtration. Indeed, when we add a sufficient amount of surfactant ( $c \gg cmc^*$ ) the hydrophobic aggregates break thanks to the screening of the CE hydrophobic flexible chains by surfactant molecules. This leads to a decrease of the aggregates size and thus to an increase of the final fraction of fluid outlet and a decrease of the viscosity, which highlights the role of the hydrophobic associations in the increase of the CE solution viscosity. Finally, it shows that the number and the size of the aggregates play a major role in the solution viscosity as well as in the filtration process.

### Concluding Remarks

By means of different filtration experiments and a wide range of characterization techniques, we have attempted at explaining macroscopic observations associated with the constraint flow of CE solutions. Our main conclusions, which reflect consistent findings from all experiments, are summarized below:

Given a preparation protocol, CE solutions (here, methyl (hydroxyethyl) cellulose) cannot molecularly disperse, but instead comprise of highly polydisperse aggregates at all scales (from a few hundred of nanometers to a hundred micrometers). These aggregates evolve in time.

Hydrophobic associations appear to be responsible for the formation of the aggregates, which in turn play the key role in the increase of solution viscosity and the enhancement of its viscoelasticity. In parallel, a sharp decrease of the solution viscosity signals the addition of surfactant. Conversely, the larger aggregates (of about several microns to hundred microns) have a semicrystalline structure which relates to natural cellulose.

The accumulation of aggregates on the sieve mesh leads to jamming (obstruction of the pores) which explains the clogging observed in the filtration test.

Furthermore, the soft and deformable nature of the aggregates appears to play an important role in the jamming and unjamming phenomena observed in the filtration tests.

## Acknowledgments

Partial support from the EU (FP7 infrastructure ESMT, GA-262348) is gratefully acknowledged. The authors thank Professor Ulrich Jonas (Universität Siegen, Germany) for the GPC analysis.

## Literature Cited

1. Brumaud C. *Microscopic Origins of the Rheological Consequences of Adding Cellulose Ethers in a Cementitious Suspension*. PhD Thesis. Paris: University of Paris Est, 2011. (in French).
2. Brumaud C, Bessaies-Bey H, Mohler C, Baumann R, Schmitz M, Radler M, Roussel N. Cellulose ethers and water retention. *Cem Concr Res*. 2013;53:176–184.
3. Patural L, Marchal P, Govin A, Grosseau P, Ruot B, Devès O. Cellulose ethers influence on water retention and consistency in cement-based mortars. *Cem Concr Res*. 2011;41:46–55.
4. Rubinstein M, Colby RH. *Polymer Physics*. Oxford: Oxford University Press, 2003.
5. Clasen C, Kulicke WM. Determination of viscoelastic and rheological material functions of water-soluble cellulose derivatives. *Prog Polym Sci*. 2001;26:1839–1919.
6. Bülichen D, Kainz J, Plank J. Working mechanism of methyl hydroxyethyl cellulose (MHEC) as water retention agent. *Cem Concr Res*. 2012;42:953–959.
7. Jenni A, Zurbriggen R, Holzer L, Herwegh M. Changes in microstructures and physical properties of polymer-modified mortars during wet storage. *Cem Concr Res*. 2006;36:79–90.
8. Marlière C, Mabrouk E, Lamblot M, Coussot P. How water retention in porous media with cellulose ethers works. *Cem Concr Res*. 2012;42:1501–1512.
9. Arvidson SA, Lott JR, McAllister JW, Zhang J, Bates FS, Lodge TP, Sammler RL, Li Y, Brackhagen M. Interplay of phase separation and thermoreversible gelation in aqueous methylcellulose solutions. *Macromolecules*. 2013;46:300–309.
10. Joshi SC. Sol-Gel behavior of hydroxypropyl methylcellulose (HPMC) in ionic media including drug release. *Materials*. 2011;4:1861–1905.
11. Roe RJ, Bachetta VL, Wong PMG. Refinement of pendent drop method for the measurement of surface tension of viscous liquid. *J Phys Chem*. 1967;71:4190–4193.
12. Chevalier T, Chevalier C, Clain X, Dupla JC, Canou J, Rodts S, Coussot P. Darcy's law for yield stress fluid flowing through a porous medium. *J Non-Newtonian Fluid Mech*. 2013;195:57–66.
13. Callaghan PT. *Principles of Nuclear Magnetic Resonance Microscopy*. Oxford: Oxford Science Publications, 1995.
14. Whitaker S. Flow in porous media I: a theoretical derivation of Darcy's law. *Transp Porous Media*. 1986;1:3–25.
15. Washburn EW. The dynamics of capillary flow. *Phys Rev*. 1921;17:273.
16. Bohren CF, Huffman DR. *Absorption and Scattering of Light by Small Particles*. New York: Wiley, 1998.
17. Berne BJ, Pecora R. *Dynamic Light Scattering*. New York: Dover, 2000.
18. Provencher SW. CONTIN: a general purpose constrained regularization program for inverting noisy linear algebraic and integral equations. *Comput Phys Commun*. 1982;27:229–242.
19. Burchard W. Solubility and solution structure of cellulose derivatives. *Cellulose*. 2003;10:213–225.
20. Medronho B, Lindman B. Competing forces during cellulose dissolution: from solvents to mechanisms. *Curr Opin Colloid Interface Sci*. 2014;19:32–40.
21. Bodvik R. *Bulk and Interfacial Properties of Cellulose Ethers*. Ph.D. Thesis. Stockholm: Royal Institute of Technology, 2012.
22. Keary CM. Characterization of METHOCEL cellulose ethers by aqueous SEC with multiple detectors. *Carbohydr Polym*. 2001;45:293–303.
23. Morgenstern B, Kammer HW. On the particulate structure of cellulose solutions. *Polymer*. 1999;40:1299–1304.
24. Yathindra C, Rao VSR. Configurational studies of polysaccharide chains. Part II: cellulose. *Biopolymers*. 1970;9:783–790.
25. Lott JR, McAllister JW, Wasbrough M, Sammler RL, Lodge TP, Bates FS. Fibrillar structure in aqueous methylcellulose solutions and gels. *Macromolecules*. 2013;46:9760–9771.
26. Tande BM, Wagner NJ, Mackay ME, Hawker CJ, Jeong M. Viscometric, hydrodynamic and conformational properties of dendrimers and dendrons. *Macromolecules*. 2001;34:8580–8585.
27. Thuresson K, Lindman B. Association in nonionic cellulose ether solutions due to microcrystallites. *Colloids Surf A Physicochem Eng Asp*. 1999;159:219–226.
28. Mewis J, Wagner NJ. *Colloidal Suspension Rheology*. Cambridge: Cambridge University Press, 2012.
29. Roussel N, Nguyen TLH, Coussot P. Filtration is a lottery. *Phys Rev Lett*. 2007;98:114502.
30. Schulz L, Seger B, Burchard W. Structures of cellulose in solution. *Macromol Chem Phys*. 2000;201:2008–2022.
31. Esquenet C. *Structural and Dynamic Properties of Solutions of Rigid and Semi-Rigid Polyelectrolytes and Associative Polysaccharides*. Ph.D. Thesis. Grenoble: University of Joseph Fourier, 2003. (in French).
32. Kobayashi K, Huang C, Lodge TP. Thermoreversible gelation of aqueous methylcellulose solutions. *Macromolecules*. 1999;32:7070–7077.
33. Tanaka R, Meadows J, Williams PA, Phillips GO. Interaction of hydrophobically modified hydroxyethyl cellulose with various added surfactants. *Macromolecules*. 1992;25:1304–1310.

Manuscript received Nov. 18, 2014, and revision received June 16, 2015.